Modal Approximations for the Dynamics of Shape Memory Alloys Under External Thermomechanical Actions

P. Morin and R. D. Spies

Programa Especial de Matemática Aplicada (PEMA)
CONICET - Universidad Nacional del Litoral
Güemes 3450 - 3000 Santa Fe - ARGENTINA

Departamento de Matemática
Facultad de Ingeniería Química
Universidad Nacional del Litoral

Keywords: Shape Memory Alloys, hysteresis, conservation laws, initial-boundary value problem, modal approximations.

Abstract

In this article an algorithm for numerically solving the non-linear system of partial differential equations (PDEs) that model the dynamics of martensitic phase transitions in one-dimensional Shape Memory Alloys is presented. The algorithm is based upon a state-space formulation of the equations. The approximations are defined in terms of the eigenvalues and eigenvectors of the operator associated to the linear part of the resulting semilinear Cauchy problem. For the alloy $Au_{23}Cu_{30}Zn_{47}$ numerical results are shown under the effect of different external distributed actions and for several initial conditions.

1 Introduction

In this article we consider the following one-dimensional non-linear initial-boundary value problem (IBVP):

$$\begin{aligned}\rho u_{tt} - \beta\rho u_{xxt} + \gamma u_{xxxx} = \\ f(x,t) + \left(2\alpha_2(\theta-\theta_1)u_x - 4\alpha_4 u_x^3 + 6\alpha_6 u_x^5\right)_x, \\ x \in (0,1),\ 0<t<T, \quad (1)\end{aligned}$$

$$\begin{aligned}C_v\theta_t - k\theta_{xx} = g(x,t) + 2\alpha_2\theta u_x u_{xt} + \beta\rho u_{xt}^2, \\ x\in(0,1),\ 0<t<T, \quad (2)\end{aligned}$$

$$\begin{aligned}u(x,0)=u_0(x),\ u_t(x,0)=v_0(x),\ \theta(x,0)=\theta_0(x), \\ x\in(0,1), \quad (3)\end{aligned}$$

$$\begin{aligned}u(0,t)=u(1,t)=u_{xx}(0,t)=u_{xx}(1,t)=0, \\ 0\le t\le T, \quad (4)\end{aligned}$$

$$\theta_x(0,t)=\theta_x(1,t)=0, \quad 0\le t\le T \quad (5)$$

where the subscripts "x" and "t" denote partial derivatives. Equations (1) to (5) arise from the conservation laws governing the thermomechanical processes taking place in a one-dimensional unit-length Shape Memory Alloy (SMA). These processes are characterized by solid–solid phase transitions (martensitic transformations). Equations (1) and (2) reflect the conservation of linear momentum and energy, respectively. The functions and variables present in Eqns. (1) to (5) have the following physical meaning: $u(x,t)$ = transverse displacement, $\theta(x,t)$ = absolute temperature, ρ = mass density, C_v = specific heat, k = thermal conductivity coefficient, β = viscosity constant, $f(x,t)$ = distributed loads (input),

depend on the material being considered and they appear in the free energy potential which is taken in the Landau-Ginzburg form

$$\begin{aligned}\Psi(\epsilon,\epsilon_x,\theta) = -C_v\theta\ln\left(\frac{\theta}{\theta_2}\right) + C_v\theta + C \\ + \alpha_2(\theta-\theta_1)\epsilon^2 - \alpha_4\epsilon^4 + \alpha_6\epsilon^6 + \frac{\gamma}{2}\epsilon_x^2, \quad (6)\end{aligned}$$

where $\epsilon = u_x$ is the linearized shear strain. The constants θ_1 and θ_2 in Eqn. (6) are two critical temperatures and C represents a fixed energy reference level. The body is assumed to be a simply supported unit-length beam thermally insulated at both ends.

The PDEs (1) and (2) are coupled and nonlinear due to the terms coming from the partial derivatives of the free energy. For a detailed account of the origin of these equations see the work by Spies (1995) and the referenes therein.

Although there are several representations for the free energy potential of SMA materials (Falk 1980, 1983; Songmu, 1989; Songmu and Sprekels, 1989; Sprekels, 1989a), the form of Eqn. (6) seems to be the simplest one which is able to reproduce several phenomena -such as hysteresis, shape memory and superelasticity- observed in real SMA materials under different external thermomechanical actions. For values of θ close to θ_1, Ψ is a nonconvex function of ϵ and the stress-strain laws obtained from Eqn. (6) are strongly temperature-dependent (see Fig. 1). At low temperatures these curves exhibit an elasto-plastic behavior at small loads and a second elastic branch at large loads, which permits the body to withstand forces beyond the plastic yield, after which, subsequent unloading produces residual deformation. In the intermediate temperature range the behavior is superelastic, also called pseudoelastic. Here, a plastic yield is also found. However, loading beyond this plastic yield followed by complete unloading does not lead to residual deformation.

beyond a certain critical value. Finally, in the high temperature range the behavior is almost linearly elastic with a modulus of elasticity which increases with temperature. Hysteresis loops are observed in the stress-strain curves at low and at intermediate temperatures (Spies, 1995, and the references therein).

It is known that certain alloys exhibit a much more complicated behavior. For example, certain CuZnAl alloys show strain hardening and nested hysteresis loops (Muller and Xu, 1991). Although these phenomena can be captured in an isothermal and static setting (Spies, 1996), it is not yet clear how they can be included into the dynamic equations (1) and (2).

Due to their unique characteristics SMA have found a broad spectrum of applications such as orthodontic and other dental devices, heat engines, temperature switches and fuses, pipe coupling devices (Funakubo, 1987), hybrid composites (Rogers *et al.*, 1989) and several interesting applications in Medicine (Castleman *et al.*, 1976; Funakubo, 1987; Schmerling *et al.*, 1975).

Since the discovery of NiTinol (a Nikel-Titanium alloy) by Buehler (Malloy, 1990) in 1962 several mathematical models were proposed and studied (Achenbach and Muller, 1982, 1983; Falk 1980, 1983; Muller, 1979; Muller and Villaggio, 1977; Muller and Wilmanski, 1980; Wilmansky, 1983). Most of this models, however, were static and did not take into account the strong coupling between the mechanical and thermal properties, which is one of the distinguishing features possessed by SMA. It was not until recent years that mathematical models were able to deal with most of the unusual properties of SMA and, at the same time, to allow for the inclusion of boundary and distributed external actions that can be used as control variables (Niezgodka and Sprekels, 1988, 1991; Songmu, 1989; Songmu and Sprekels, 1989; Spies, 1995; Sprekels, 1989a, 1989b). This article follows a state-space approach introduced recently (Spies, 1995).

2 State-Space Formulation and Preliminaries

In this section we shall formulate the initial-boundary value problem of Eqns. (1) to (5) as an abstract semilinear Cauchy problem in an appropriate Hilbert space, and we shall briefly recall some preliminaries which will be needed later on.

We define the state space Z as the Hilbert space $H_0^1(0,1)\cap H^2(0,1)\times L^2(0,1)\times L^2(0,1)$ with the inner product

$$\left\langle \begin{pmatrix} u \\ v \\ \theta \end{pmatrix}, \begin{pmatrix} \tilde{u} \\ \tilde{v} \\ \tilde{\theta} \end{pmatrix} \right\rangle \doteq \gamma \int_0^1 u''(x)\overline{\tilde{u}''(x)}\,dx + \rho \int_0^1 v(x)\overline{\tilde{v}(x)}\,dx + \frac{C_v}{k}\int_0^1 \theta(x)\overline{\tilde{\theta}(x)}\,dx.$$

Next, the operator A on Z is defined by

$$D(A) = \left\{ \begin{pmatrix} u \\ v \\ \theta \end{pmatrix} \middle| \begin{array}{l} u \in H^4(0,1), \\ u(0) = u(1) = u''(0) = u''(1) = 0 \\ v \in H_0^1(0,1)\cap H^2(0,1) \end{array} \right\},$$

and for $z = \begin{pmatrix} u \\ v \\ \theta \end{pmatrix} \in D(A)$,

$$A \begin{pmatrix} u \\ v \\ \theta \end{pmatrix} \doteq \begin{pmatrix} 0 & I & 0 \\ -\frac{\gamma}{\rho}D^4 & \beta D^2 & 0 \\ 0 & 0 & \frac{k}{C_v}D^2 \end{pmatrix} \begin{pmatrix} u \\ v \\ \theta \end{pmatrix},$$

where $D^n \doteq \frac{\partial^n}{\partial x^n}$.

We assume that the functions $f(x,t)$ and $g(x,t)$ satisfy the following hypothesis.

(H1) For each fixed $t \geq 0$, the functions $f(x,t)$ and $g(x,t)$ are in $L^2(0,1)$ and there exist nonnegative functions $K_f(x)$ and $K_g(x) \in L^2(0,1)$ such that

$$|f(x,t_1) - f(x,t_2)| \leq K_f(x)|t_1 - t_2|,$$

and

$$|g(x,t_1) - g(x,t_2)| \leq K_g(x)|t_1 - t_2|,$$

for all $x \in (0,1)$, and $t_1, t_2 \in [0,T]$.

We also define $z_0(x) = \begin{pmatrix} u_0(x) \\ v_0(x) \\ \theta_0(x) \end{pmatrix}$ and $F(t,z) : \mathbb{R}_0^+ \times Z \to Z$ by

$$F(t,z) = \begin{pmatrix} 0 \\ f_2(t,z) \\ f_3(t,z) \end{pmatrix},$$

where

$$\begin{aligned} \rho f_2(t,z)(x) &= f(x,t) \\ &\quad + \left(2\alpha_2(\theta-\theta_1)u_x - 4\alpha_4 u_x^3 + 6\alpha_6 u_x^5\right)_x, \\ C_v f_3(t,z)(x) &= g(x,t) + 2\alpha_2\theta u_x v_x + \beta\rho v_x^2. \end{aligned}$$

With the above notation, the IBVP of Eqns. (1) to (5) can be formally written as the following semilinear Cauchy problem in the Hilbert space Z:

$$(\mathcal{P}) \begin{cases} \dfrac{d}{dt}z(t) = Az(t) + F(t,z), & 0 \leq t \leq T, \\ z(0) = z_0 \end{cases}. \tag{7}$$

The following results follow immediately from theorems 3.7 and 3.11 of Spies (1995) with only slight modifications accounting for the slightly different boundary conditions being considered here. Since the modifications needed are trivial we do not give details here.

Theorem 2.1. (Spies, 1995) Let $A : D(A) \subset Z \to Z$ as previously defined. Then the set of eigenvalues $\sigma_p(A)$ of the operator A is given by

$$\sigma_p(A) = \{\lambda_n^+\}_{n=1}^\infty \cup \{\lambda_n^-\}_{n=1}^\infty \cup \{\alpha_n\}_{n=0}^\infty,$$

where

$$\lambda_n^{+,-} = \sqrt{\mu_n}\left(-r \pm \sqrt{r^2-1}\right), \quad \alpha_n = -\frac{k}{C_v}n^2\pi^2$$

and

$$\mu_n = \frac{\gamma n^4 \pi^4}{\rho} \quad \text{and} \quad r = \frac{\beta\sqrt{\rho}}{2\sqrt{\gamma}}.$$

The corresponding eigenvectors in Z are, respectively,

$$\begin{pmatrix} \sin(\pi n x) \\ \lambda_n^+ \sin(\pi n x) \\ 0 \end{pmatrix}_{n=1,2,\cdots}, \quad \begin{pmatrix} \sin(\pi n x) \\ \lambda_n^- \sin(\pi n x) \\ 0 \end{pmatrix}_{n=1,2,\cdots},$$

and $\begin{pmatrix} 0 \\ 0 \\ \cdots \end{pmatrix}$.

Also, the operator A generates an analytic semigroup of contractions $T(t)$ on Z.

Theorem 2.2 (Local existence of solutions). (Spies, 1995) Let A be as defined above. Then, for any initial data $z_0 \in D(A)$, there exists $t_1 = t_1(z_0)$ such that the IVP $(\mathcal{P})$ has a unique classical solution $z(t) \in C([0,t_1) : Z) \cap C^1((0,t_1) : Z)$.

3 Finite Dimensional Approximations

In this section finite-dimensional modal approximations to solutions of problem $(\mathcal{P})$ are defined. For fixed $N \in \mathbb{N}$ let

$$\beta_n^N(x) \doteq \begin{pmatrix} \sin \pi n x \\ \lambda_n^+ \sin \pi n x \\ 0 \end{pmatrix}, \quad \beta_{N+n}^N(x) \doteq \begin{pmatrix} \sin \pi n x \\ \lambda_n^- \sin \pi n x \\ 0 \end{pmatrix},$$

$$\text{and} \quad \beta_{2N+n}^N(x) \doteq \begin{pmatrix} 0 \\ 0 \\ \cos \pi (n-1) x \end{pmatrix},$$

for $n = 1, 2, \cdots, N$, where $\lambda_n^{+,-}$ are as in Theorem 2.1, and let us define Z^N to be the span of $\hat{\beta}_N \doteq \{\beta_n^N(x)\}_{n=1}^{3N}$ endowed with the Z-norm. Then $\bigcup_{N=1}^{\infty} Z^N$ is dense in Z and, since the β_n^N's are eigenvectors of A, it follows that Z^N is invariant under A. Note also that Z^N is itself a Hilbert space.

Next, we define the finite-dimensional approximating problem $(\mathcal{P}^N)$ in Z^N, as follows:

$$(\mathcal{P}^N) \begin{cases} \dfrac{d}{dt} z^N(t) = A^N z^N(t) + F^N(t, z^N(t)), & 0 \le t \le T \\ z^N(0) = P^N z_0 \end{cases},$$

where $P^N : Z \to Z^N$ is the orthogonal projection of Z onto Z^N, A^N is the restriction of A to Z^N and $F^N(t,z) \doteq P^N F(t,z)$. The density of $\bigcup_{N=1}^{\infty} Z^N$ in Z implies the strong convergence of P^N to the identity.

Since Z^N has finite dimension, the operator A^N on Z^N is bounded and linear, and a fortiori, it generates a uniformly continuous semigroup of bounded linear operators $T^N(t)$ on Z^N.

The following results on local existence of solutions of problem $(\mathcal{P}^N)$ and their convergence to the solution of $(\mathcal{P})$ can be found in the work by Morin and Spies (1996).

Theorem 3.1. (Morin and Spies, 1996) Let $z_0 \in Z$. Then, for any positive integer N, there exists $t_1^N > 0$ such that $(\mathcal{P}^N)$ has a unique classical solution on $[0, t_1^N)$.

Theorem 3.2. (Morin and Spies, 1996) Let $z_0 \in D(A)$. Suppose that $z^N(t)$ and $z(t)$ are solutions of $(\mathcal{P}^N)$ and $(\mathcal{P})$, respectively, and let $[0, t_1)$ be the maximal interval of existence of $z(t)$. Then, for any $t_1' < t_1$, there exists a constant N_0 such that $z^N(t)$ exists on $[0, t_1']$ for every $N \ge N_0$ and $\|z^N(t) - z(t)\|_Z \to 0$ for every $t \in [0, t_1']$.

Next we shall find the representation of the approximating problem $(\mathcal{P}^N)$ in the basis $\hat{\beta}_N$ of Z_N. For this purpose, let w^N be the vector whose components are the coefficients of the solution $z^N(t) = \begin{pmatrix} u^N(t) \\ \cdots \end{pmatrix}$ of $(\mathcal{P}^N)$ in the basis $\hat{\beta}_N$

Then $w^N(t)$ is the solution of the IVP

$$\left(\tilde{\mathcal{P}}^N\right) \begin{cases} \dot{w}^N(t) = \tilde{A}^N w^N(t) + \tilde{F}^N\left(t, w^N(t)\right) \\ w^N(0) = w_0^N \end{cases},$$

with

$$\begin{aligned} \tilde{A}^N &= \left(Q^N\right)^{-1} K^N, \\ \tilde{F}^N(t,w) &= \left(Q^N\right)^{-1} R^N F\left(t, Q^N w\right) \\ &= \left(Q^N\right)^{-1} R^N \begin{pmatrix} 0 \\ f_2(t, Q^N w) \\ f_3(t, Q^N w) \end{pmatrix}, \\ w_0^N &= \left(Q^N\right)^{-1} R^N \begin{pmatrix} u_0 \\ u_1 \\ \theta_0 \end{pmatrix}, \end{aligned}$$

where the matrices Q^N, K^N and the mapping $R^N : Z^N \to \mathbb{R}^{3N}$ are defined by

$$\left(Q^N\right)_{i,j} = \langle \beta_i^N, \beta_j^N \rangle, \qquad \left(K^N\right)_{i,j} = \langle \beta_i^N, A^N \beta_j^N \rangle,$$
$$\left(R^N z\right)_i = \langle \beta_i^N, z \rangle.$$

$i, j = 1, 2, \cdots, 3N$.

4 Description of the Algorithm

In this section the matrices Q^N, K^N and the mapping $R^N : Z^N \to \mathbb{R}^{3N}$ are constructed. We will later use them to evaluate the linear and nonlinear part of the equation.

The matrix Q^N turns out to be

$$Q^N = \begin{bmatrix} Q_1^N & Q_2^N & 0 \\ Q_3^N & Q_4^N & 0 \\ 0 & 0 & Q_5^N \end{bmatrix}$$

where Q_k^N, $k = 1, 2, \cdots, 5$ are all $N \times N$ diagonal matrices and, for every $n = 1, 2, \cdots, N$

$$\begin{aligned} \left(Q_1^N\right)_{n,n} &= \frac{\gamma n^4 \pi^4 + \rho \left|\lambda_n^+\right|^2}{2}, \\ \left(Q_2^N\right)_{n,n} &= \frac{\gamma n^4 \pi^4 + \rho \lambda_n^+ \overline{\lambda_n^-}}{2}, \\ \left(Q_3^N\right)_{n,n} &= \left(\overline{Q_2^N}\right)_{n,n}, \\ \left(Q_4^N\right)_{n,n} &= \frac{\gamma n^4 \pi^4 + \rho |\lambda_n^-|^2}{2}, \end{aligned}$$

and

$$Q_5^N = \operatorname{diag}\left\{1, \frac{1}{2}, \frac{1}{2}, \cdots, \frac{1}{2}\right\}.$$

Taking into account that, being β_n^N eigenfunctions of A, for $n = 1, 2, \ldots, 3$,

$$\begin{aligned} A\beta_n^N &= \lambda_n^+ \beta_n^N, \\ A\beta_{n+N}^N &= \lambda_{(n)}^- \beta_{n+N}^N, \\ A\beta_{n+2N}^N &= -\frac{k}{C_v}(n-1)^2 \pi^2 \beta_{n+2N}^N, \end{aligned}$$

it turns out that $K^N = Q^N E^N$, where E^N is a $3N \times 3N$ diagonal matrix whose elements are given by

$$\begin{aligned} \left(E^N\right)_{n,n} &= \lambda_n^+, \\ \left(E^N\right)_{n+N,n+N} &= \lambda_{(n)}^-, \end{aligned}$$

$n = 1, 2, \dots, N$. In particular, since $\tilde{A}^N = \left(Q^N\right)^{-1} K^N$ we have that $\tilde{A}^N = E^N$.

To evaluate the nonlinear term $\tilde{F}(t, w)$ of the equation, we first reconstruct u, u_x, u_{xx}, v, v_x, θ and θ' from the vector of coefficients w on a 101-point regular grid and evaluate f_2 and f_3 on that grid.

The computation of $\left(R^N z\right)_n = \langle \beta_n^N, z \rangle$, is made through numerical integration using the Simpson's rule with a step-size of 10^{-2}.

We first used an explicit fourth order Runge-Kutta method. Due to the nonlinearities of the system this method was found to be very unstable and inefficient. The efficiency of the numerical algorithm was greatly improved using a hybrid implicit-explicit Euler method which ensures stability for much larger step sizes. Basically, this method consists of approximating the linear part of $\frac{d}{dt}z(t)$ in an implicit way while an explicit form is used for the nonlinear part. More precisely, the following time discretization scheme was used:

$$w_0^N = \gamma^N,$$

$$\frac{1}{\Delta t}\left(w_{k+1}^N - w_k^N\right) = \tilde{A}^N w_{k+1}^N + \tilde{F}^N\left(k\Delta t, w_k^N\right),$$

$k = 0, 1, \dots$.

5 Numerical Experiments

In this section numerical results obtained using the finite dimensional approximating scheme introduced in the previous sections are presented. We shall make use of the parameter values reported by Falk (1980) for the alloy $Au_{23}Cu_{30}Zn_{47}$: $\alpha_2 = 24\,J\,cm^{-3}\,K^{-1}$, $\alpha_4 = 1.5 \times 10^5\,J\,cm^{-3}$, $\alpha_6 = 7.5 \times 10^6\,J\,cm^{-3}\,K^{-1}$, $\theta_1 = 208^0\,K$, $C_v = 2.9\,J\,cm^{-3}\,K^{-1}$, $k = 1.9\,w\,cm^{-1}\,K^{-1}$, $\rho = 11.1\,g\,cm^{-3}$, $\beta = 1$, $\gamma = 10^{-12}\,J\,cm^{-1}$. Figure 1 shows the stress-strain curves obtained from the potential defined by Eqn. (6) used with these parameter values. The doted lines indicate the unstable parts of the curves, while the horizontal lines indicate possible hysteresis loops.

For the numerical results presented below we used the hybrid method described above with $N = 32$ and $\Delta t = 10^{-5}$.

5.1 Experiment 1: Low-temperature steady-state

For this experiment we took $f = g \equiv 0$, $\theta_0(x) \equiv 200^0$ K and $u_0(x) = P^N h(x)$, where

$$h(x) = \begin{cases} 0.05x, & \text{if } 0 \le x \le 0.5, \\ 0.05(1-x), & \text{if } 0.5 \le x \le 1, \end{cases}$$

and $v_0 \equiv 0$. Thus, the beam is initially in the low temperature range composed of two segments of martensites, namely, martensite M_+ on $0 \le x < \frac{1}{2}$ and martensite M_- on $\frac{1}{2} < x \le 1$ (5% initial strain). The evolution of displacement and temperature can be observed in Figs. 2a and 2b, respectively. This evolution is due to the fact that the initial condition $z_0(x) = \begin{pmatrix} u_0(x) \\ v_0(x) \\ \theta_0(x) \end{pmatrix}$ does not correspond to a steady-state of the system of Eqns. (1) to (5). The system evolves until a steady-state corresponding to two symmetric segments of martensites M_+ and M_- ($\cong 11.25\%$ strain) and to a constant temperature $\theta \cong 222^0$ K is reached. Figure 2c

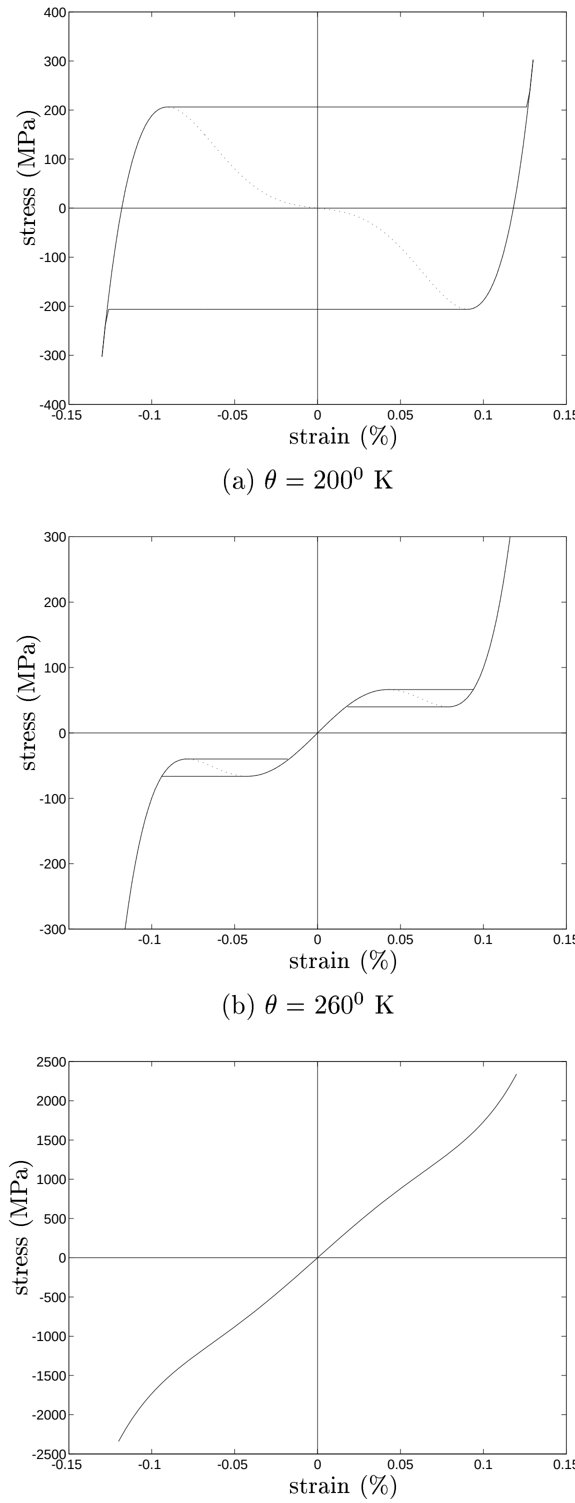

(a) $\theta = 200^0$ K

(b) $\theta = 260^0$ K

(c) $\theta = 600^0$ K

Figure 1: Stress-Strain curves for different temperatures obtained from Eqn. (6) used with the values of α_2, α_4, α_6 and θ_1 reported by Falk (1980). The dotted lines represent unstable parts of the curves. Horizontal lines indicate possible hysteresis loops.

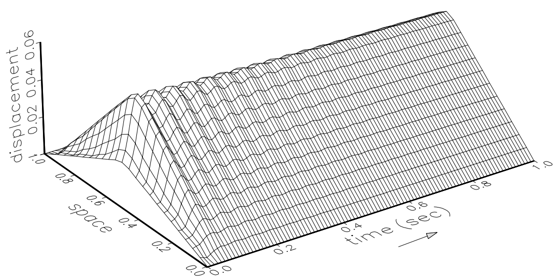

(a)

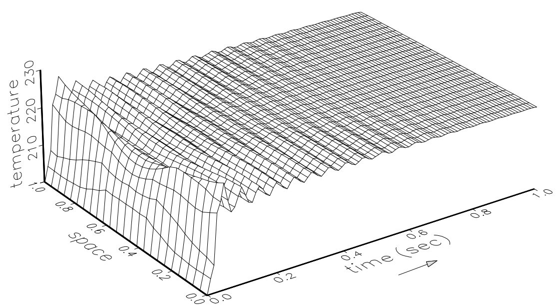

(b)

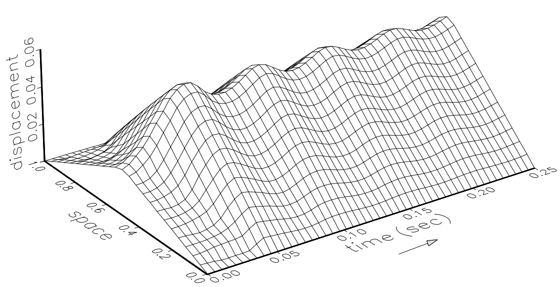

(c)

Figure 2: *Low temperature steady-state.* Evolution of displacement (a, c) and temperature (b) from an unsteady low temperature initial condition.

5.2 Experiment 2: High-temperature steady-state

Here we took $\theta_0(x) \equiv 600^0$ K and u_0, v_0, f and g as in Experiment 1. The evolution of displacement and temperature is shown in Fig. 3a and 3b, respectively. The beam oscillates until the steady-state defined by a zero deformation and a constant temperature $\theta \cong 505.6^0$ K is reached. This is in agreement with the fact that above the austenite-finish temperature $\theta = A_f$ (in this case $A_f \cong 283^0$ K) the steady-states satisfy the Eqns. $u \equiv 0$ and $\theta \equiv const$. Due to the high-temperature unsteady initial condition the beam immediately bends downward approaching the state $u \equiv 0$ while the temperature decreases slightly, originating the damped oscillations observed in Figs. 3a and 3b. The oscillations of the middle-point of the beam are shown in Fig. 3c.

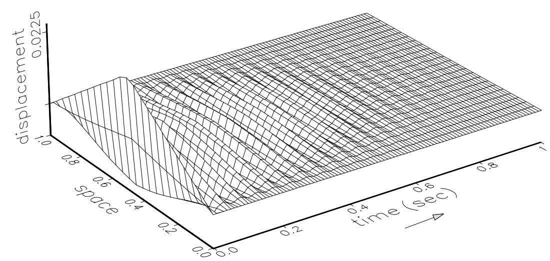

(a)

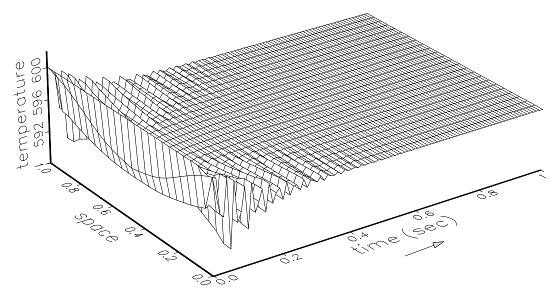

(b)

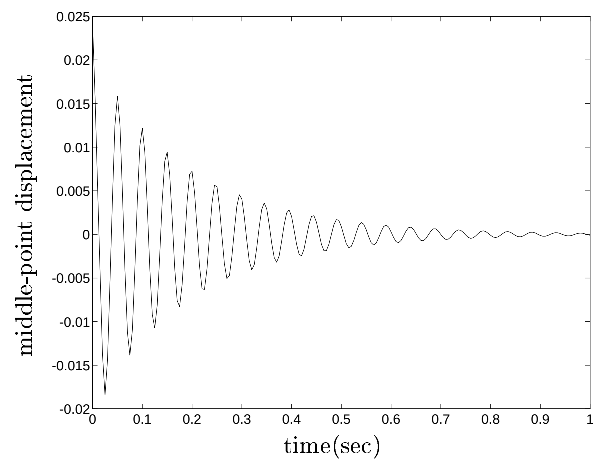

(c)

Figure 3: *High temperature steady-state.* (a) displacement profile; (b) temperature profile; (c) middle-point displacement.

5.3 Experiment 3: Pulse at low temperature

In this experiment we studied the effects of a distributed finish temperature $\theta = M_f \cong 208^0$ K. We took $u_0(x) = v_0(x) \equiv 0$, $\theta_0(x) \equiv 200^0$ K, $g(x,t) \equiv 0$ and

$$f(x,t) = \begin{cases} 5 \times 10^4, & \text{if } 0.4 \le x \le 0.6 \\ & \text{and } 0 < t < 0.5 \times 10^{-3}, \\ 0, & \text{otherwise.} \end{cases}$$

Initially, points around the center move upward while the effect of the pulse propagates to the endpoints of the beam (Figs. 4a and 4c). At exactly the time at which this effect reaches the endpoints, the middle-point deflection reaches a maximum. Then, small damped oscillations begin to take place (Fig. 4c) around the final equilibrium state which corresponds to two symmetric segments of martensites M_+, M_- ($\cong$ 11.05% strain) and to a constant temperature $\theta \cong 226^0$ K (Fig. 4b).

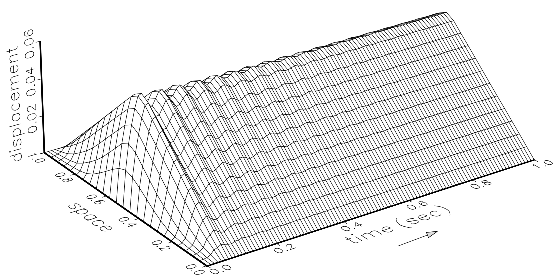

(a)

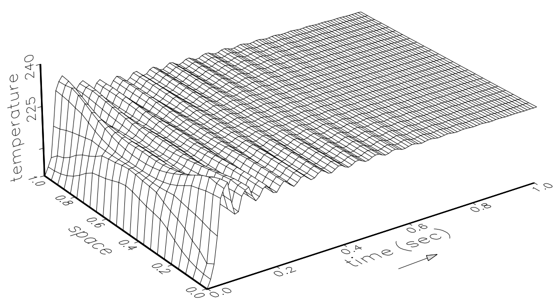

(b)

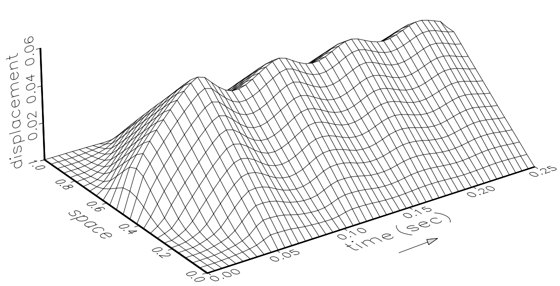

(c)

Figure 4: *Pulse at low temperature.* (a), (c) displacement profile; (b) temperature profile.

5.4 Experiment 4: Pulse at high temperature

In this case we investigated the effects of a pulse around the middle-point of the beam, which was set initially at a constant temperature above A_f. We took $\theta_0(x) \equiv 600^0$ K and u_0, v_0, f and g as in Experiment 3. At the beginning, the

These oscillations take place around the final equilibrium state defined by $u \equiv 0$ and by a constant temperature $\theta \cong 602^0$ K (Figs. 5a and 5b). Recall that above the austenite finish temperature the only unloaded steady-state is $u \equiv 0$.

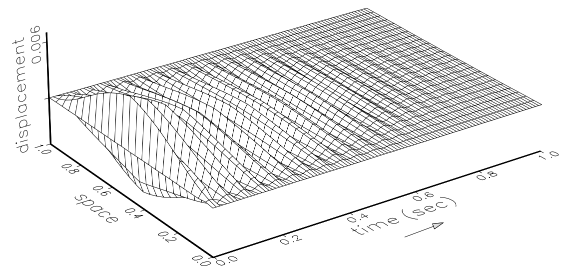

(a)

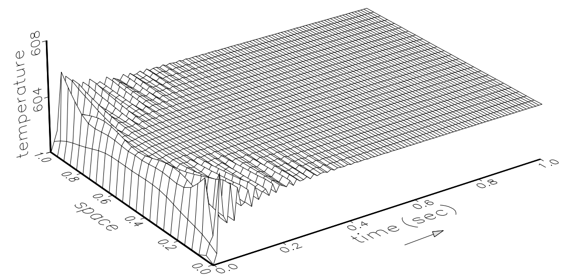

(b)

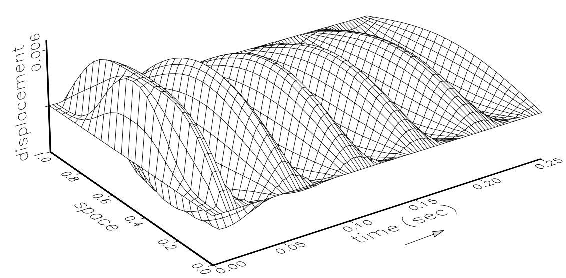

(c)

Figure 5: *Pulse at high temperature.* (a), (c) displacement profile; (b) temperature profile.

5.5 Experiment 5: Waiting-Heating

Here, we observed the effects of heating the beam when it is set initially at an equilibrium state corresponding to two symmetric segments of martensites M_+ and M_-. For this, we took as the initial data the final steady-state of Experiment 1 (11.25 % initial strain, $\theta_0(x) \equiv 222^0$ K), $f(x,t) \equiv 0$ and the heat source $g(x,t)$ consisting of a uniformly spatially distributed heat pulse as follows

$$g(x,t) = \begin{cases} 5 \times 10^4, & \text{if } 0.2 < t < 0.25, \\ 0, & \text{otherwise.} \end{cases}$$

The system remains at the initial state until the heat pulse is switched on. At this time the temperature starts to increase (Fig. 6b), the martensite crystals are converted into austenite and the beam bends downward showing small damping oscillations around zero deformation (Fig. 6a).

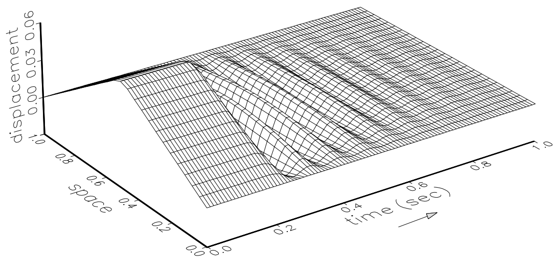

(a)

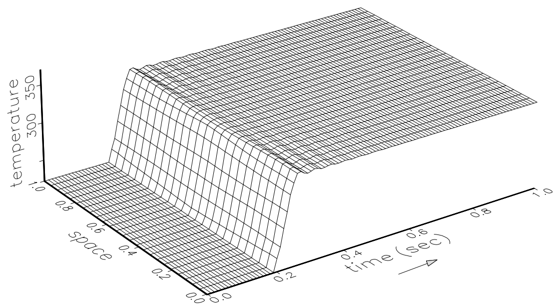

(b)

Figure 6: *Waiting-Heating.* (a) displacement and (b) temperature profiles.

5.6 Experiment 6: Heating-Waiting-Cooling (Two-way shape memory effect)

For this experiment we took again as initial data the final steady-state of Experiment 1. We also took $f(x,t) \equiv 0$ and the distributed heat source $g(x,t)$ consisting of an initial uniformly distributed heat pulse which is switched off after $t = 0.05$ sec. At $t = 1.45$ sec. the opposite heat pulse is applied until $t = 1.50$ sec. when it is switched off. More precisely,

$$g(x,t) = \begin{cases} 8 \times 10^3, & \text{if } t < 0.05, \\ -8 \times 10^3, & \text{if } 1.45 < t < 1.50, \\ 0, & \text{otherwise.} \end{cases}$$

The temperature raises uniformly up to nearly 336^0 K while the beam approaches the undeformed state. After the heat pulse is switched off, the temperature remains at about 336^0 K while the displacement shows small damped oscillations around $u \equiv 0$ due to inertial effects. The sample is now completely in the austenite phase. At $t = 1.45$, when the opposite pulse is applied, the temperature decreases uniformly and remains at about 222^0 K, while the beam undergoes a process of reverse transformation. This process takes the beam back to the original initial configuration showing the so-called two-way shape memory phenomenon (Figs. 7a to 7d).

6 Conclusions

In this article, discrete spectral or modal approximations to the nonlinear partial differential equations that model the dynamics of thermomechanical martensitic transformations in one-dimensional shape memory alloys with non-convex Landau-Ginzburg potentials were developed.

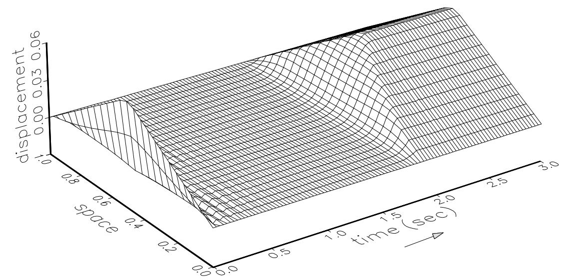

(a)

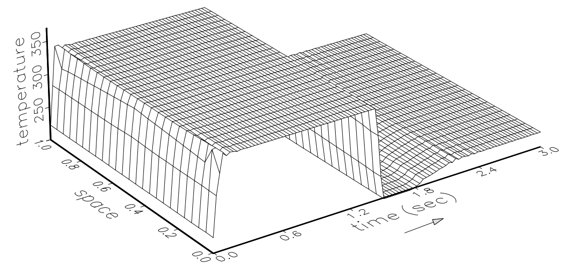

(b)

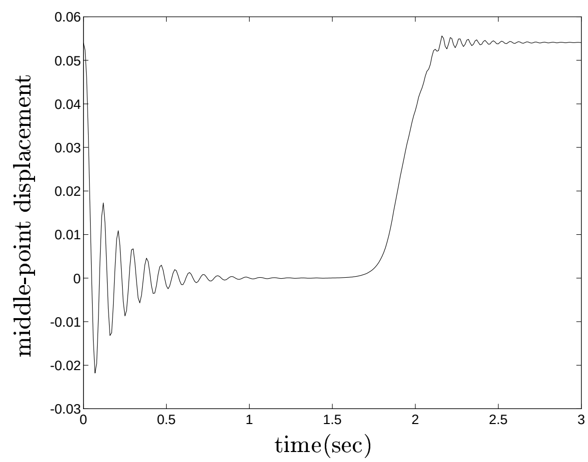

(c)

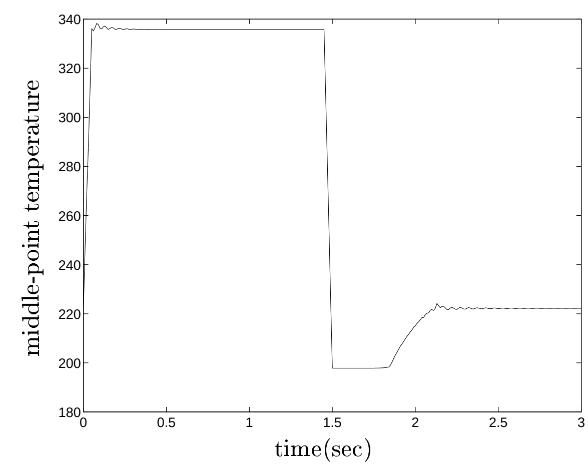

(d)

Figure 7: *Heating-Waiting-Cooling.* (a) displacement profile; (b) temperature profile; (c) middle-point displacement; (d) middle-point temperature.

external actions the model defined by Eqns. (1) to (5) is able to produce solutions whose qualitative behavior is found to be in close agreement with laboratory experiments performed on Shape Memory Alloys under similar conditions.

From a practical point of view it would be very important to find the values of the parameters that "best fit" experimental data for a given alloy. This is called the parameter identification problem about which no results are yet known. In this regard the scheme presented here provides a friendly mathematical framework for attacking this problem. Efforts in this direction are already underway and results will be published in a forthcoming article.

Acknowledgements:

The work of the authors was supported in part by CONICET, Consejo Nacional de Investigaciones Científicas y Técnicas of Argentina, UNL, Universidad Nacional del Litoral, Santa Fe, through projects CAI+D 94-0016-004-023, 96-00-017-113, and Fundación Antorchas of Argentina.

Pedro Morin was also supported by the Air Force Office of Scientific Research of U.S.A. under grants F49620-93-1-0280 and F49620-96-1-0329 while he was a visiting scientist at the Air Force Center for Optimal Design and Control, Virginia Polytechnic Institute and State University, Blacksburg, VA 24061-0531 (U.S.A.).

The authors wish to express their gratitude to the Interdisciplinary Center for Applied Mathematics of Virginia Tech, Blacksburg, and in particular to Prof. Terry Herdman, for providing the computing facilities where the codes where run.

References

Achenbach M. and I. Muller, "A Model for Shape Memory", *Jurnal de Physique*, Colloque C4, Supplément au No 12, **43**, 163–167 (1982).

Achenbach M. and I. Muller, "Creep and Yield in Martensitic Transformations", *Igenieur-Archiv* **53**, 73–83 (1983).

Castleman L. S., S. M. Motzkin, F. P. Alicandri and V. L. Bonawit, "Biocompatibility of Nitinol Alloy as an Implant Material", *Journal of Biomedical Materials Res.* **10**, 695–731 (1976).

Falk F., "Model Free Energy, Mechanics and Thermodynamics of Shape Memory Alloys", *Acta Metallurgica* **28**, 1773–1780 (1980).

Falk F., "One Dimensional Model of Shape Memory Alloys", *Arch. Mech.* **35**, 63–84 (1983).

Funakubo H. (Ed.), *Shape Memory Alloys*, Precision Machinery and Robotics, Vol. 1, Translated from the Japanese by J. B. Kennedy, Gordon and Breach Science Publishers, New York (1987).

Malloy E. C., "Nitinol Provides Shape Memory Capabilities", *On the Surface Magazine*, 22 June 1990.

Morin P. and R. D. Spies, "Convergent Spectral Approxi- Institute for Mathematics and its Applications, University of Minnesota, accepted for publication in *Journal of Nonlinear Analysis: Theory, Methods and Applications* (1996).

Muller I., "A Model for a Body with Shape Memory", *Arch. Rational Mechanics Anal.* **70**, 61–67 (1979).

Muller I. and P. Villaggio, "A model for an Elastic-Plastic Body", *Arch. Rational Mechanics Anal.* **65**, 25–46 (1977).

Muller I. and K. Wilmanski, "A model for Phase Transitions in Pseudoelastic Bodies", *Il Nuovo Cimento* **57B**, 283–318 (1980).

Muller I. and H. Xu, "On the Pseudo-Elastic Hysteresis", *Acta Metall.* **39**, 263–271 (1991).

Niezgodka M. and J. Sprekels, "Existence of Solutions for a Mathematical Model of Structural Phase Transitions in Shape Memory Alloys", *Mathematical Methods in the Applied Sciences* **10**, 197–223 (1988).

Niezgodka M. and J. Sprekels, "Convergent Numerical Approximations of the Thermomechanical Phase Transitions in Shape Memory Alloys", *Numer. Math.* **58**, 759–778 (1991).

Rogers C., C. Liang and J. Jia, "Behavior of Shape Memory Alloy Reinforced Composites, Part I: Model Formulations and Control Concepts", 30^{th} *AIAA/ASME/ASCE/AHS/ASC Structures, Structural Dynamics and Materials Conference*, Mobile, Alabama, 2011–2017 (1989).

Schmerling M. A., M. A. Wilkow, A. E. Sanders and J. E. Woosley, "A Proposed Medical Application of the Shape Memory Effect: A NiTi Harrington Rod for the Treatment of Scoliosis", in *Shape Memory Effects in Alloys*, Jeff Perkins (Ed.), Plenum Press, New York, 563–574 (1975).

Songmu Z., "Global Solutions to the Thermomechanical Equations with Non-convex Landau-Ginzburg Free Energy", *Journal of Applied Mathematics and Physics (ZAMP)* **40**, 111–127 (1989).

Songmu Z. and J. Sprekels, "Global Solutions to the Equations of a Ginzburg-Landau Theory for Structural Phase Transitions in Shape Memory Alloys", *Physica D* **39**, 59–76 (1989).

Spies R. D., "A State-Space Approach to a One-Dimensional Mathematical Model for the Dynamics of Phase Transitions in Pseudoelastic Materials", *Journal of Mathematical Analysis and Applications* **190**, 58–100 (1995).

Spies R. D., "An Algorithm for Simulating the Isothermal Hysteresis in the Stress-Strain Laws of Shape Memory Alloys", *Journal of Materials Science* **31**, 6631-6636 (1996).

Sprekels J., "Automatic Control of One-Dimensional Thermomechanical Phase Transitions", in *Mathematical Models for Phase Change Problems*, International Se-

Sprekels J., "Global Existence for Thermomechanical Processes with Nonconvex Free Energies of Ginzburg-Landau Form", *Journal of Mathematical Analysis and Applications* **141**, 333–348 (1989b).

Wilmansky K., "Propagation of the Interface in Stress-Induced Austenite-Martensite Transformation", *Ingenieur-Archiv.* **53**, 291–301 (1983).